Applied Thermal Engineering 185 (2021) 116433

Contents lists available at ScienceDirect

Applied Thermal Engineering

journal homepage: www.elsevier.com/locate/apthermeng

Experimental investigation of air-conditioning and HDH desalination hybrid system using new packing pad humidifier and strips-finned helical coil

S.A. Nada [a,b,*], A. Fouda [c], M.A. Mahmoud [a], H.F. Elattar [a]

[a] Department of Mechanical Engineering, Benha Faculty of Engineering, Benha University, Benha 13511, Qalyubia, Egypt
[b] Egypt-Japan University of Science and Technology, New Borg El-Arab City 21934, Alexandria, Egypt
[c] Department of Mechanical Power Engineering, Faculty of Engineering, Mansoura University, 35516 El-Mansoura, Egypt

ARTICLE INFO

Keywords:
HDH system
Cooling pad humidification
Stripped fins helical coil
Water desalination
Operating conditions

ABSTRACT

A low energy HDH (humidification-dehumidification) and AC (air-conditioning) hybrid system using an efficient design of dehumidifier (strips-finned helical coil) and packing pad material (cellulose paper in bee-hive structure) is proposed. An experimental investigation of the performance of the proposed system is conducted for wide ranges of air and water flow rates and temperatures and packing pad thickness. The results showed that (i) the proposed hybrid system can produce fresh water and remove space cooling load to maintain the required comfort conditions, (ii) the fresh water production rate, cooling load capacity and the system performance increase with increasing air and water flow rates and temperatures and cooling pad thickness, (iii) the proposed HDH system with the new humidification-dehumidification sections has better productivity and performance compared to other systems, (vi) daily production cost of the system increases with increasing inlet air and water flow rates and decreasing cooling pad thickness and air and water temperatures, and (v) production cost per kg of fresh water decreases by increasing cooling pad thickness and air and water flow rates and temperatures. The system performance parameters (fresh water productivity, cooling load capacity, space supply air temperature and coefficient of performance) can reach to 17.42 kg/h, 3.9 kW and 16 °C, and 4.35, respectively. Moreover, the lowest specific cost of fresh water production can be obtained is 0.7 ¢/kg_{FW}, respectively. Finally, empirical correlations of system productivities and performance parameters in terms of operating conditions and system geometric parameters were predicted within acceptable errors.

1. Introduction

With increasing world population, water shortage became a worldwide problem in many hot regions; at the same time, there is great requests for air conditioning of buildings for thermal comfort. In these regions un-efficient traditional systems were separately used for fresh water production and air-conditioning. Currently, many investigators presented hybrid AC and HDH water desalination systems and others utilized solar energy for energy saving.

Nowadays, the water shortage is a worldwide problem, where about seven hundred million people suffer from potable water accessibility [1]. Additionally, the problem of water deficiency increases with raising the world population; for example and according to the statistics after ten years the world demands of potable water will be 6900 billion m^3 that exceeds the available amount by 2400 billion m^3 [2]. Several studies have been conducted to obtain clean water from salt water (seas & oceans) using different techniques of water desalination including VC (vapor-compression), ME (multi-effect), RO (reverse-osmosis), MSF (multi-stage flash), and HDH (humidification-dehumidification) desalination systems. All of these technologies except HDH are high energy consuming and too expensive, accordingly they are only appropriate for medium and high capacities. HDH technique is less energy consuming and cost effective for small capacities, where it was found that HDH technique consumes about 150 kJ per kg of fresh water and consumed about 3.5 L fuel per $m^3$of fresh water [3].

Fresh water production by HDH system is widely used for the sake of fresh water production with minimum driving energy. Extra energy in the air and water heating can be used in this system for productivity enhancement. Fresh water productivity of HDH systems depends on the

* Corresponding author at: Department of Mechanical Engineering, Benha Faculty of Engineering, Benha University, Benha 13511, Qalyubia, Egypt.
E-mail addresses: sameh.nada@ejust.edu.eg, samehnadar@yahoo.com (S.A. Nada).

https://doi.org/10.1016/j.applthermaleng.2020.116433
Received 13 April 2020; Received in revised form 3 October 2020; Accepted 2 December 2020
Available online 6 December 2020

Nomenclature

c_p	specific heat at constant pressure, kJ/kg K
G	standard gravitational acceleration, m/s^2
H_P	circulating pump head, m
h	specific enthalpy, kJ/kg
$\dot{m}$	mass flow rate, kg/s
$\dot{Q}_R$	space cooling load, kW
q	specific heat losses, kJ/kg
t	temperature, ^{o}C
T	absolute temperature, K
$\dot{W}_{comp}$	power consumption of the compressor, kW
$\dot{W}_{fan}$	power consumption of the air fan, kW
$\dot{W}_{pump}$	power consumption of the water pump, kW

Greek symbols

δ	Packing pad thickness, mm
ΔP_a	system air pressure drop, Pa
ΔP_w	humidifier water pressure drop, Pa
ε_{hum}	humidifier effectiveness
ε_{coil}	cooling coil effectiveness
η	Saturation efficiency, $\eta = [(t_1\text{-}t_2)/(t_1\text{-}t_{wb,1})] \times 100$
P	density, kg/m^3
ω	specific humidity ratio of moist air (mass basis), kg_v/kg_a

Subscripts

O	ambient air state
1	humidifier inlet state
2	humidifier outlet state
3	dehumidifier outlet state
A	air/dry air
cond	condensate
coil	cooling coil
evap	evaporated
H	heater
hum	humidifier
in	inlet
out	outlet
V	water vapor
W	water
Wb	Wet bulb
R	room
R,cyc	refrigeration cycle
Sys	system

Abbreviations

COP	coefficient of performance
HDH	Humidification-dehumidification
TOC	Total operating cost, $/day
SCFWP	Specific Cost of Fresh Water Production, [¢/kg_{FW}]

effectiveness of the system components. Humidifier and dehumidifying coil effectiveness strongly affect the productivity of the HDH system. The efficiency of the dehumidifying coil depends on the geometry and orientation of the coil, while the effectiveness of the humidifier section depends on the air to water contact and wettability conditions. The operating conditions such as air and water flow rates and temperatures and air humidity also strongly affect the system productivity.

Several types of humidifiers are widely used in HDH systems, e.g. spray towers [4], bubble-columns [5], and packed-bed towers [6]. Narayan et al. [7] proved that the effectiveness of the packed-bed tower is high due to the high air to water contact time and contact area. Kabeel and El-said [8] studied experimentally a hybrid SSF (single stage flashing) and HDH system using polyvinyl chloride packed bad humidifier. Later, Kabeel et al. [9] experimentally compared the performance of solar assisted HDH system using free and forced draft air circulation in cellulose paper packed-column humidifier. The effects of air circulation directions (up, up-down, down) were investigated on the system performance. The results revealed that down air circulation has higher performance than other circulation arrangements. Kabeel et al. [10], in another study, reviewed and showed that the HDH desalination technique is the most suitable one for small capacity fresh water productivity. HDH can operates at low temperatures and the total necessary thermal energy can be attained from solar energy or waste heat. Moreover, increasing the evaporator and condenser surface areas enhances the system productivity [11-13].

Dai et al. [14] constructed a HDH unit using packing pad humidifier to improve the performance and unit productivity. It was found that the unit performance mainly depends on the humidifier entry water temperature, seawater and air flow rates. Moreover, the unit thermal efficiency reached to 85% with the possibility of using waste energy to drive the unit. Al-Enezi et al. [15] constructed an HDH unit including plastic packed pad humidifier. They studied the influence of water and air temperatures and flow rates at humidifier inlets on heat and vapour transfer coefficients. It was observed that the highest productivity is obtained at high and low water temperatures at humidifier and dehumidifiers inlets, respectively. Nawayseh et al. [16] compared mass transfer coefficients of different wooden slats packing-pads (wooden slats) with previously used packing types. They reported that the coefficient mainly depends on packing material. Muthusamy and Srithar [17] experimentally studied HDH fresh water productivity for different modifications. Sawdust and gunny bag packed-pad were used to improve water evaporation. The results revealed that the modified system significantly enhances system productivity per input power. Yamalı and Solmus [18] experimentally investigated the influence of operating and geometric conditions on the performance of HDH system using plastic material packing pad. It was found that the water productivity increases with raising both of entry water and cooling water flow rates and wasn't influenced with increasing air mass flow rate.

Orfi et al. [19] proved experimentally and numerically the existence of optimum mass flow rate ratio that gives maximum productivity of the HDH system. Al-Hallaj et al. [20] presented experimental investigation to evaluate productivity of HDH system using wooden packing pad. They reported that the system productivity is higher than that of single-basin stills system. Moreover, it was reported that higher air temperatures with higher forced circulation have slightly impact on the system performance.

Ahmed et al. [21] experimentally investigated the performance of HDH system using corrugated aluminum sheets packing pad humidifier with finned tube condenser in the dehumidifier under different operating parameters. The results showed the increase of the productivity with increasing humidifier and dehumidifier water flow rates and humidifier inlet temperature. The water productivity increased from 10.0 to 15.0 L/h with decreasing dehumidifier water temperature from 28.50 °C to 17.0 °C and fresh water cost was about 0.01 $/L. He et al. [22] proposed theoretically an open air and water HDH system using a packing bed humidifier driven by industrial waste heat to enhance the system thermal and economic performances. The results showed that the maximum production, GOR and SEC were 96.450 kg/ h, 1.700 and 0.380 kWh/ kg, respectively. He et al. [23] theoretically investigated and optimized HDH system by coupling the open air-open water HDH system with a heat pump. The results demonstrated that the best system performances parameters are: 89.27 kg/h for water productivity, 4.17 for GOR and 0.016 $/L for fresh water cost. Nada et al. [24] investigated experimentally the performance of direct evaporative cooling using

cellulose papers in bee-hive structure packing pad based on energy-exergy concept. The experiments were conducted at different pad thicknesses and operating variables to study the performance of the cooling pad. New empirical correlations were presented to predict the performance parameters for any operating conditions.

Many HDH water desalination systems integrated with vapor compression systems were presented by many researchers to enhance the overall system performance. Aly et al. [25] presented experimental and theoretical investigation on the performance of MVC (mechanical vapour-compression) desalination system for different operating temperatures. Younes et al. [26] proposed a modified HDH system named HC (Humidification Compression) for the enhancement of the system performance. Al-Enezi et al. [15] studied the characteristics of HDH system at different temperatures. The results showed that the highest productivity was at high inlet temperature and low flow rate of humidifier water and low temperature of dehumidifier water. Giwa et al. [27] investigated the performance of small scale hybrid HDH and solar PV thermal recovery system under Abu Dhabi, UAE weather conditions. Kabeel and El-Said [28] carried out comparison investigation of different arrangements of solar assisted hybrid HDH and single flashing system. Gao et al. [29] conducted an analysis for heat and mass transfer between air and water flows in the humidifier of HDH system. Mehrgoo and Amidpour [30] used the constructed theory for conceptual design of humidification-dehumidification (HDH) desalination unit and showed that the main design features of a direct contact HDH desalination process can be determined based on the method of the constructed design.

Several researchers conducted investigations of integrating the HDH system with solar systems [31-38]. Mohamed and El-Minshawy [31] theoretically investigated the performance of solar assisted HDH system and conducted a parametric study to the effects of the operating conditions on the system productivity and performance. Ghazal et al. [32] constructed a compact size solar assisted HDH prototype to enhance the system performance. Nafey et al. [33] presented a theoretical study of the solar assisted HDD by developing a mathematical model to simulate the HDD system and study the effects of the operating conditions on the system performance for different configurations of the system. Nafey et al. [34] experimentally investigated the effects of water and air flow rates on the performance of a solar assisted HDH system under the Suez City, Egypt weather conditions. Abdel Dayem and Fatouh [35] theoretically and experimentally investigated the performance of different configurations of solar assisted HDH systems to identify the system of the best performance. Yıldırım and Solmus [36] theoretically investigated the performance of solar assisted HDH for Antalya, Turkey. Sharshir et al. [37] experimentally investigated the performance of a continuous HDH system coupled with evacuated-tube solar-collector and solar still. Recently, Fouda et al. [38] conducted the performance investigation of a developed solar-HDH water desalination systems for hot and humid climate cities.

Water desalination consumes huge amount of energy. Also, considerable amount of energy is consumed to drive the air conditioning systems, especially in hot/humid areas. Different techniques were proposed to reduce the energy consumptions of water desalination and air conditioning systems by integrating the two systems together. Hybrid air conditioning-HDH systems were proposed and discussed by many investigators to enhance systems performance and productivity and to reduce energy consumption. Nada et al. [39] proposed four configurations of A/C-HDH hybrid systems for hot and dry climates. Different arrangements of evaporative cooler and heat recovery units were tested at different operating conditions. Later, Nada et al. [40] achieved an experimental study to investigate the performance of an A/C-HDH hybrid system using vapor-compression refrigeration unit under different operating parameters. Results showed the improvement of the system performance with the increase of per air humidity and flow rate. Yuan et al. [41] investigated the performance of air-conditioning and HDH desalination hybrid system driven by heat pump using mathematical modeling. Fouda et al. [42] proposed innovated solar assisted HDH-AC hybrid system for hot and humid climates. The hourly and daily performance parameters of the systems for a wide range of operating and design conditions. Elattar et al. [43] conducted a theoretical parametric study for the performance and economic study of a hybrid A/C-HDH solar assisted system. Nada et al. [44] recently proposed and evaluated a hybrid energy-efficient A/C-HDH system for high latent load buildings/spaces.

Based on the above literature review, although there is some works integrated the vapor compression AC system with HDH water desalination system, there is a lack of works that integrate AC-HDH hybrid system for low energy space cooling (i.e. maintaining human thermal comfort) and fresh water production. Such systems are not completely investigated experimentally; especially with new and efficient system components. So, in the present paper, a proposed low energy HDH and AC hybrid system using an efficient new design of dehumidifier (strips-finned helical coil) and a novel packing pad material humidifier (cellulose paper in bee-hive structure) is presented. The new dehumidifier design (strips-finned helical coil) is compact and has better heat and mass transfer characteristics in vertical orientation as compared to straight tubes heat exchangers [13]. Moreover, the novel pad material has higher thermal–hydraulic performance if compared to another available pad materials [45] that justifies the novelty of the present work when they integrated together in a whole hybrid system for AC and HDH water desalination. The proposed system is experimentally investigated to evaluate the system performance at different operating and geometric conditions. The impacts of air and seawater inlet conditions and packing pad material thickness on the proposed system performance parameters are investigated. Economic analysis of the proposed system is also conducted. The study also aims to deduce empirical correlations for the prediction of the system productivity and performance parameters in terms of all studied parameters.

2. Experimental facility and measuring instruments

The experimental setup was designed and constructed to study the performance of the proposed hybrid HDH water desalination and AC system at different ranges of operating and geometric conditions including air flow rate, humidifier water flow rate, humidifier water temperature and humidifier packing pad thickness. The study aims to propose new HDH-AC hybrid system using new humidifier-packing pad type and new design dehumidifier finned coil to maximize the system performance and its water productivity. The cold air exit from the system is used to provide the cooling and comfort conditions inside the space required to be air conditioned.

2.1. Experimental setup

To characterize the behavior of the proposed HDH-AC hybrid system, the system was tested in steady-state conditions using subsonic rectangular wind tunnel system of dimensions 0.39 m × 0.335 m cross section with 3 m long as illustrated in Fig. 1. The duct of the wind tunnel is made of 0.8 mm thick galvanized sheet steel. The duct system includes the following sections: air supply section, air heating section, humidifying section (new packing pad type), and dehumidifying section (new design finned helical coil). The air exit from the system is used the supply cooling air for a room as shown in the figure. Measuring instruments are used to measure the required parameters (temperatures, relative humidity, and flow rates). The experimental setup can be considered consisting of four main loops (air, saline water, refrigerant, and fresh water loops).

In the air loop, air is extracted from surrounding using air supply section then the air flows over the air heating section to be heated using three electric heaters of 3.0 kW each placed in staggered-arrangement (see Fig. 2). The air is then passes in an air mixer (see Fig. 2) to maintain uniform velocity, temperature, and humidity of air in the duct. The

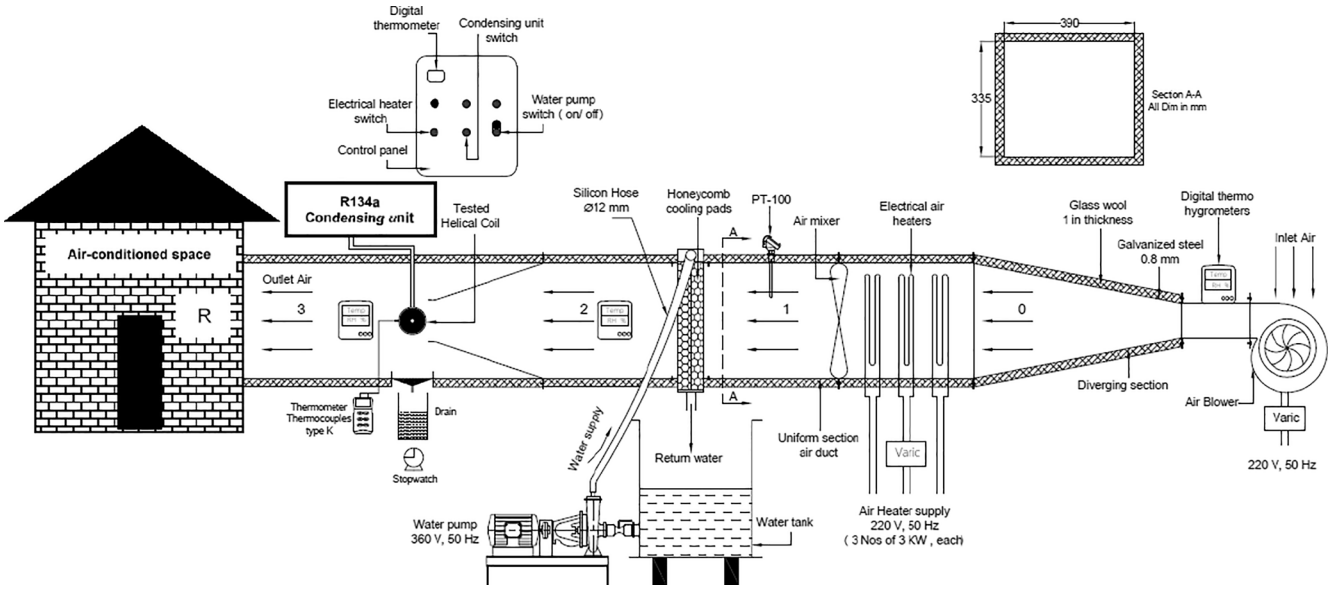

Fig. 1. Schematic of the experimental setup.

air then flows through the packing pad humidifier where it is humidified using a water cooling system. Finally, the humid air is dehumidified when it passes over the outer surface of the finned helical cooling and dehumidifying coil. The air is then supplied to the space required to be air conditioned to remove its cooling load and maintain it at the required comfort conditions. In the saline water loop, the slain water temperature is firstly adjusted in the saline water tank using a controlled electric heater. The water is then pumped from the tank to the humidifying section to a water distributer where water is sprayed over the packing pads in cross flow with the air that passes in the air duct causing air humidification.

The humidifying section consists of water supply unit including circulation pump, control valve, water tank, electric heater, water spray and packing pads (new type, bee-hive structure as shown in Fig. 3). In the water loop, a water pump of 10 L/min capacity is used, and a control valve is installed downstream the pump to control water flow rate. The water tank is fabricated from galvanized steel of 0.8 mm thickness and 400 × 335 × 390 mm dimensions. The water tank comprises an electrical heater (1.5 kW) formed in serpentine shape and controlled by a variac to adjust the spray water temperature. The configuration and detailed dimensions of the humidifying section is shown in Fig. 3.

The air flow rate in the system is adjusted using variac (variable transformer) to drive fan and very its speed according to the input voltage. The air exit temperature from the heater was controlled by another variac (variable transformer) connected to the heater to control the input voltage to the electric heater.

In the saline water loop, the slain water temperature is firstly adjusted in the saline water tank using a controlled electric heater. The water is then pumped from the tank to the humidifying section to a water distributer where water is sprayed over the packing pads in cross flow with the air that passes in the air duct causing air humidification. The humidifying section consists of water supply unit including circulation pump, control valve, water tank, electric heater, water spray and packing pads (new type, bee-hive structure as shown in Fig. 3). In the water loop, a water pump of 10 L/min capacity is used, and a control valve is installed downstream the pump to control water flow rate. The water tank is fabricated from galvanized steel of 0.8 mm thickness and 400 × 335 × 390 mm dimensions. The water tank comprises an electrical heater (1.5 kW) formed in serpentine shape and controlled by a variac to adjust the spray water temperature. The configuration and detailed dimensions of the humidifying section is shown in Fig. 3.

Four packing pads were used in the experiments with 35, 70, 105 and 140 mm thicknesses. The manufacturer of the pads is Tabreed (Group company in Egypt) [46]. The used pad type is "Tabreed 45/45 Angle" with area of 0.335 × 0.390 m^2. The pads consist of corrugated sheets of cellulose which is 0.7 mm in thickness gathered in a "bee-hive" structure which generates air flow inside the cell. The pad geometric dimensions and arrangements are shown in Fig. 4.

The refrigerant loop consists of condensing unit and cooling/dehumidifier coil with refrigerant R134a as shown in Fig. 1. The loop. The model of the condensing unit is Danfoss- Optyma™. The outdoor condensing unit consists of compressor with filter drier and air-cooled condenser. The cooling/dehumidifier coil is a new design finned helical coil connected to the condensing unit through copper piping system. The coil is made of thin-aluminum tubes 8.0 mm diameter and 0.50 mm thickness. The geometric dimensions of the coil are given in Fig. 5 (b) where, d = 8.0 mm, Rc = 80.0 mm, b = 20.0 mm and the number of coil turns is 24. The fines are radially ripped externally arranged towards the coil axis on the form of flat wire strips as shown in Fig. 5 (a). The fins dimensions are 30.0 mm (length) × 2.0 mm (width) × 0.50 mm (thickness) with 0.70 mm spacing between them. The coil is oriented vertically to give better performance [13]. Air flows over the surfaces of coil and fins to be cooled and dehumidified. Water vapor in the humid flowing air condenses on coil and fins surfaces producing fresh water that is collected in the fresh water basin. Then the cooled-dehumidified air is supplied to the room to cool and maintain it at the required comfort temperature. The experimental setup photocopy is shown in Fig. 6.

2.2. Measuring instruments

The instrumentations of measuring the required parameters at different locations of the experimental set up are given in Table 1. The measuring ranges, accuracy and resolution of each instrument are also given in the table. Three hygro-thermometers, digital thermometer, digital differential pressure manometer and Pitot tube anemometer and manometer. Three hygro-thermometers were used to measure the relative humidities and temperatures at different locations in the experimental set up as shown in Fig. 1. Two of them (HTC-1) were used to measure the temperature and relative humidity of the air at the inlet and outlet of the helical coil, while the third one (SH-109) was used to measure the ambient air condition in the laboratory. PT100 temperature sensor was connected to a digital thermometer (model TC4Y) to measure the temperatures at the inlet of the humidifier. A digital differential pressure manometer (0.5 PSI, HD755) was used to measure the air

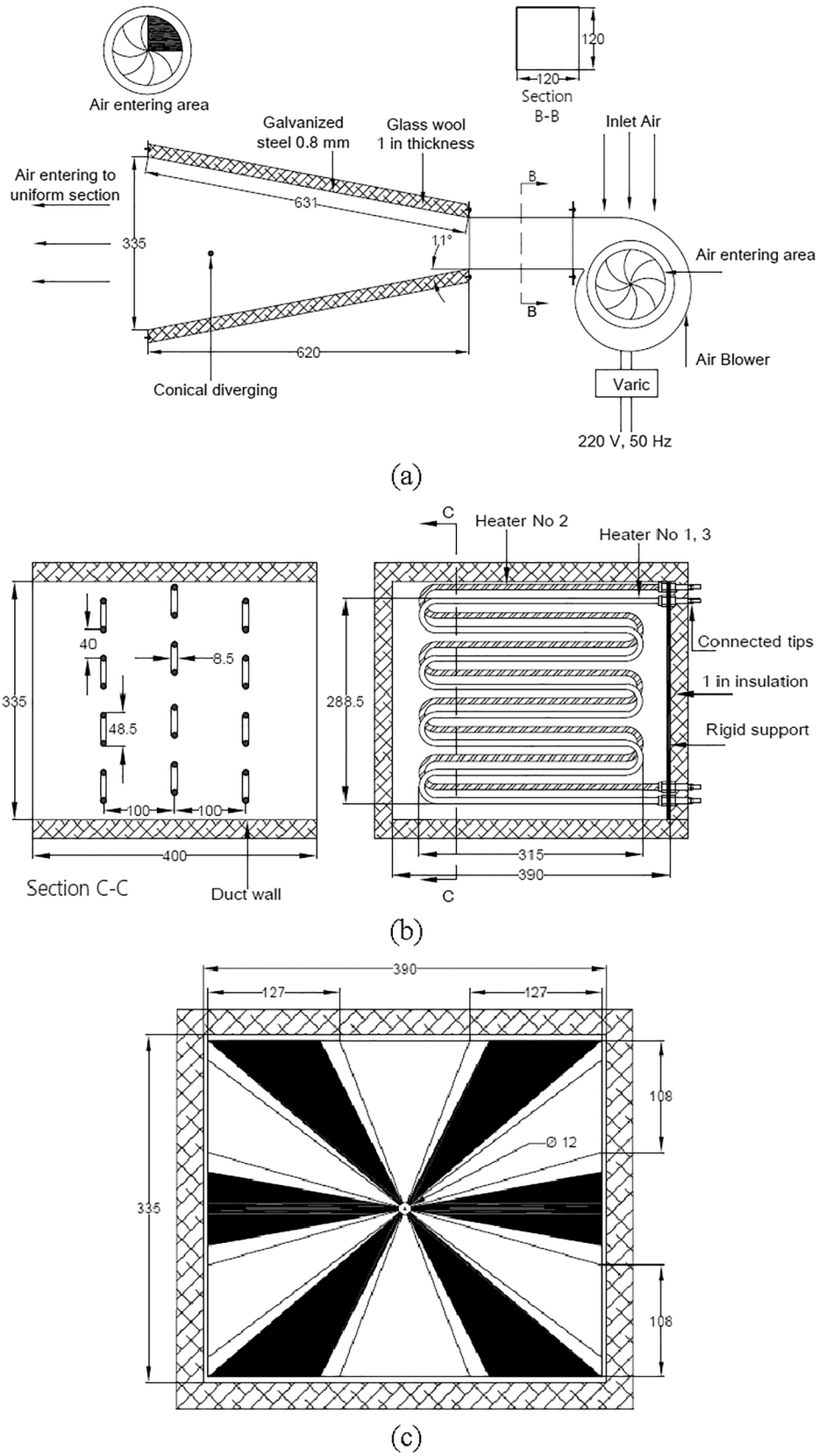

Fig. 2. Configuration and full dimensions of (a) air supply section, (b) air heaters and (c) air mixer.

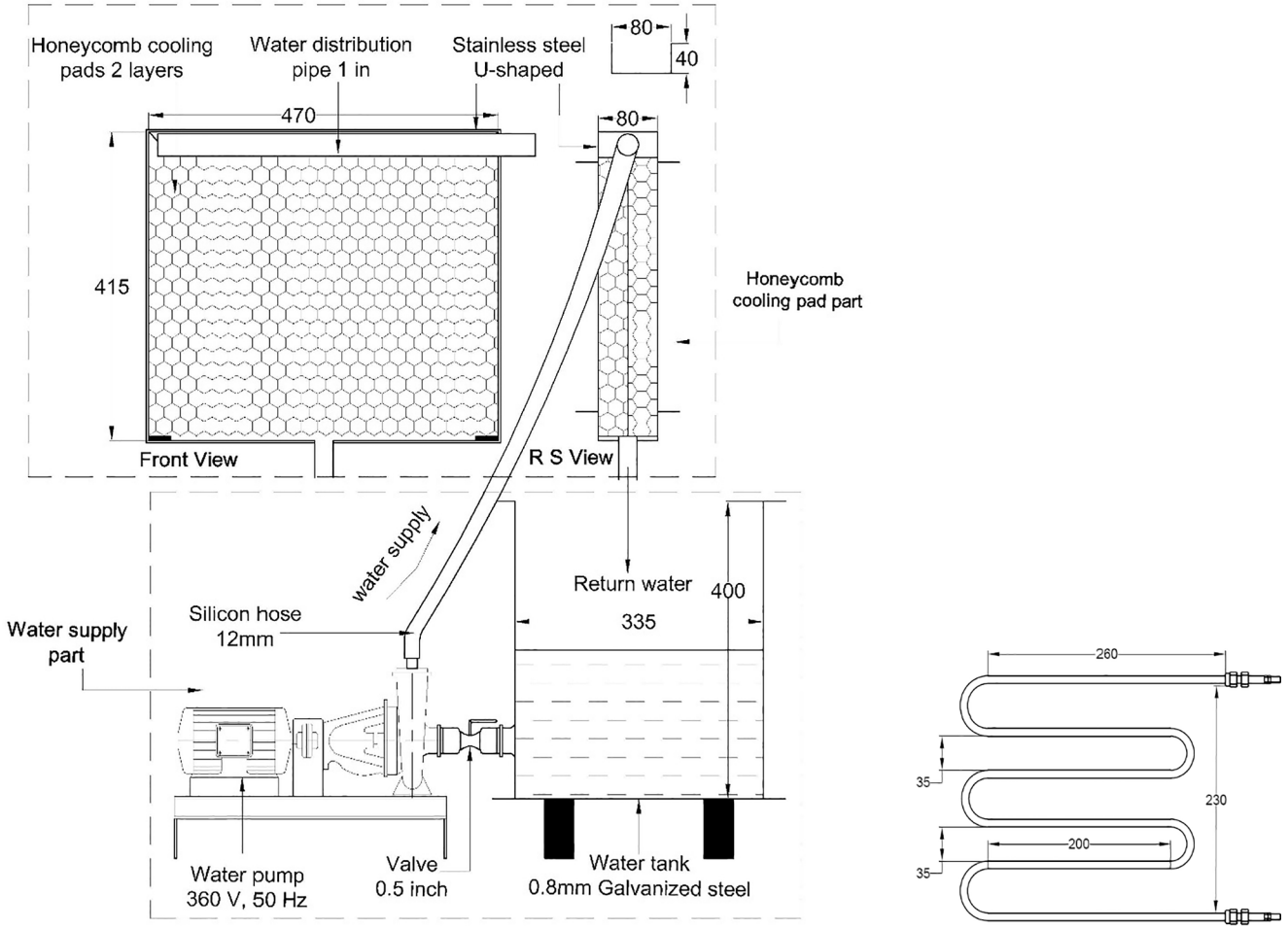

Fig. 3. Configuration and full dimensions of humidifying unit.

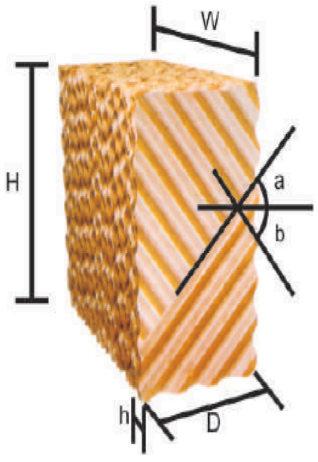

H	47 cm
W	41 cm
D	3.5 cm
a	45°
b	45°
h	7 mm

Fig. 4. Geometric dimensions and arrangements of bee-hive cellulosic pad.

Finned-helical coil

a- Photos of tested helical coils

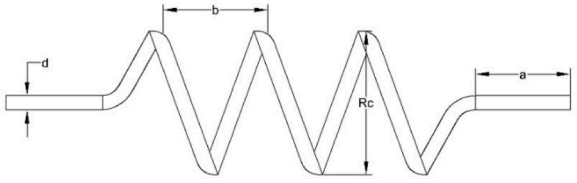

a- Dimensions of the helical coil

Fig. 5. Helical coil.

pressure drop across the humidifier. Pitot tube anemometer and manometer (HD-350) are used to measures the air velocity and airflow rate in the air duct. The detailed technical specifications of measuring instruments that used in experimental setup are tabulated in Table 1.

3. Experimental procedure, conditions, and validations

Many tests were carried out to investigate the thermal and hydro-

Fig. 6. General view of experimental setup.

Table 1
Instrumentations List and specification.

Instruments	Parameters	Ranges	Error/ Accuracy	Resolution
Hygro thermometer (Model: HTC-1)	Temperature and Relative humidity at coil inlet and exit	−50.0 to 70.0 °C, 10% to 99% RH	± 0.50 °C ± 1.0% RH	± 0.10 °C ± 0.20% RH
Hygro-thermometer (Model: SH-109)	Ambient temperature and relative humidity	−10.0 to 50.0 °C, 20.0% to 99.0% RH	± 0.50 °C ± 1.0 % RH	± 0.10 °C ± 0.20% RH
Temperature sensor (PT100) & digital thermometer (TC4Y)	Temperature at humidifier inlet	−50.0 to 400.0 °C	± 0.50 °C	± 0.10 °C
Digital differential pressure manometer 0.5 PSI (Model: HD755)	Pressure drop across cooling pads	0.0 – 0.50 Psi	±0.30%	0.001 Psi
Pitot tube anemometer & manometer (Model: HD-350)	Air velocity	1.0 to 80.00 m/ sec	±1.0%	0.010 m/s

dynamic behavior of the proposed system. The experiments were conducted at different air and water flow rates and temperatures as well as at different packing pad thickness.

Before recording any experiment data, the following procedures should be considered to confirm steady state conditions and subsequent the accuracy of readings.

- The air velocity was adjusted to maintain the required air flow rate
- The temperature of air exit from the heating section was adjusted at the required value
- The water pump flow rate was adjusted to required value using control valve.
- The water temperature of the humidifier tank was maintained to the required value.
- Waiting until steady state condition was attained.
- The condensed water (fresh water) was collected across the dehumidifier in graduated cylinder.
- The measurements were considered stable and could be recorded when their fluctuations were less than the accuracy of the sensors (i.e. less than ± 0.5 °C, ±1%, ±0.1 m/s, ±0.3% for air temperature, relative humidity, air velocity, and pressure drop, respectively).
- The above-mentioned steps were repeated to cover the ranges of the studied operating conditions listed in Table 2.

For validation of the experimental setup and procedure, preliminary experiments were conducted on commonly used reference packing pad for comparison and validation. The packing pad is (CELdek) made of cellulose paper (manufacturer: Munters company). The validation study was accomplished based on the measured saturation efficiency given by [47-51] and pressure drop across the packing pad (100 mm thickness) for different air velocities. The current data was collected and compared with different researchers [47-51]. Fig. 7 shows that the comparison of current experimental findings from our experimental setup with other authors is given reasonable agreement. Therefore, the accuracy of recent measurements is valid to perform the current study with confidence.

4. Data reduction and processing

Analysis of the characteristics and performance of the proposed AC-HDH hybrid system is conducted based on the energy and mass balances of each component of the system as follows:

Air and Water Heaters:

The energy balances through the air and water heaters can be expressed as

$$\dot{Q}_{a,h} = \dot{m}_a\, c_{p,a}\, (t_1 - t_0) \tag{1}$$

$$\dot{Q}_{w,h} = \dot{m}_w\, c_{p,w}\, \left(t_{w,out} - t_{w,in}\right) \tag{2}$$

Humidifier:

Energy and mass balances of humidifier section give:

$$\dot{m}_a\, h_1 + \dot{m}_w\, h_w - \dot{m}_a h_2 - q = 0 \tag{3}$$

$$\dot{m}_{w,evap} = \dot{m}_{makeup} = \dot{m}_a(w_2 - w_1) \tag{4}$$

The humidifier effectiveness can be found according to correlations that was presented by Narayan et al. [52], and Sharqawy et al. [53]

Table 2
Studied parameters and their values.

Parameter	Studied Range
$\dot{m}_a$	0.042–0.169 kg/s
t_1	45–65 °C
$\dot{m}_w$	0.046–0.1667 kg/s
t_w	31–37 °C
δ	35–104 mm

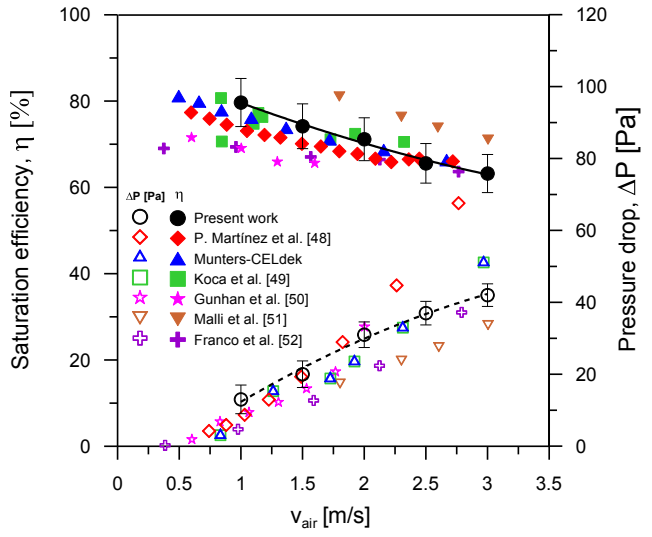

Fig. 7. Validation of the experimental setup and procedure.

$$\varepsilon_{hum} = max\left(\frac{(h_2 - h_1)}{(h_{2,ideal} - h_1)}, \frac{(h_{w,in} - h_{w,out})}{(h_{w,in} - h_{w,out,ideal})}\right) \quad (5)$$

where the ideal outlet enthalpies of air and water are calculated assuming air outlet temperature equals the inlet water temperature and water outlet temperature equals air temperature, respectively.

The power consumptions for the air fan and water pump are calculated from:

$$\dot{W}_{fan} = \frac{\dot{m}_a \Delta P_a}{\rho_a \eta_{fan}} \quad (6)$$

$$\dot{W}_{pump} = \frac{\dot{m}_w \Delta P_w}{\rho_w \eta_{pump}} \quad (7)$$

Where η_{fan} and η_{pump} are taken as 75%.

Cooling Coil:

Mass and energy conservation of the cooling coil and its effectiveness can be expressed as:

$$\dot{m}_a(h_2 - h_3) = \dot{m}_r\left(h_{r,out} - h_{r,in}\right) + \dot{m}_{cond}\, c_{p,w}\, t_{w,cond} \quad (8)$$

$$\dot{m}_{FW} = \dot{m}_{cond} = \dot{m}_a(w_2 - w_3) \quad (9)$$

$$FWR = \frac{\dot{m}_{FW}}{\dot{m}_{makeup} + \dot{m}_a w_0} \quad (10)$$

$$\varepsilon_{coil} = max\left(\frac{(h_2 - h_3)}{(h_2 - h_{3,ideal})}, \frac{(h_{r,out} - h_{r,in})}{(h_{r,out,ideal} - h_{r,in})}\right) \quad (11)$$

Where the air and refrigerant ideal outlet enthalpies are estimated based on the assumptions that the air outlet temperature is the same of the inlet refrigerant temperature and refrigerant outlet temperature is the same temperature of the air, respectively.

Capacity of cooling coil capacity, COP of the AC unit and the room cooling load removed by the supply air can be respectively expressed as:

$$\dot{Q}_{\mathrm{Ref},cyc} = \dot{m}_r(h_{r,out} - h_{r,in}) \quad (12)$$

$$COP_{\mathrm{Ref},cyc} = \frac{\dot{Q}_{\mathrm{Ref},cyc}}{\dot{W}_{comp}} \quad (13)$$

$$\dot{Q}_{\mathrm{R}} = \dot{m}_a(h_R - h_3) \quad (14)$$

The system performance parameters can be estimated based on the overall coefficient performance of the system (COP_{sys}), the total operating cost of the system (TOC) per day and the specific cost of fresh water production (SCFWP) as follows

$$COP_{sys} = \frac{\dot{m}_{FW}\, h_{fg} + \dot{Q}_R}{\dot{W}_{comp} + \dot{W}_{fan} + \dot{W}_{pump} + \dot{Q}_{a,h} + \dot{Q}_{w,h}} \quad (15)$$

$$TOC = (\dot{W}_{comp} + \dot{W}_{fan} + \dot{W}_{pump} + \dot{Q}_{a,h} + \dot{Q}_{w,h}) \times OT\,[h/day] \times EUR[\$/kWh] \quad (16)$$

$$SCFWP\,[¢/kg_{FW}] = \frac{\left(\frac{\dot{m}_{FW}\, h_{fg}}{\dot{m}_{FW}\, h_{fg} + \dot{Q}_R}\right) \times TOC}{\dot{m}_{FW}\,[kg/h] \times OT\,[h/day]} \quad (17)$$

Where the electricity unit rate (EUR, $/kWh) and operating time (OT, h/day) are taken in the present work as 0.05 $/kWh and 12 h/day, respectively. The performance analysis of the hybrid A/C-HDH system is investigated by solving Eqs. 1–17 by using Engineering Equation Solver software (EES).

Uncertainty analysis:

The uncertainty analysis is estimated for the obtained results based on the errors of the measurements of hygro-thermometer, digital thermometer and Pitot tube anemometer. Therefore, it is important to estimate the effect of the errors of these measurements on the system performance parameters such as $\dot{m}_{FW}$, FWR, COP_{sys}, $\dot{Q}_R$, ε_{coil}, ε_{hum}, TOC and SCFWP. The methods were presented by Mofatt [54] to find the uncertainty of measured and calculated experimental results are using in the present work.

$$w_Y = \left[\left(\frac{\partial Y}{\partial X_1} w_1\right)^2 + \left(\frac{\partial Y}{\partial X_2} w_2\right)^2 + \cdots\cdots + \left(\frac{\partial Y}{\partial X_N} w_n\right)^2\right]^{0.5} \quad (18)$$

where Y is the considered variable, $(X_1, X_2, X_3, \ldots, X_n)$ are the set of measured parameters, w_Y is the total uncertainty, δX_1, δX_2, $\ldots..\delta X_n$ are the uncertainty of the measured variables and $\frac{\partial Y}{\partial X_i}$ is calculated by numerical differentiation. The results of the minimum and maximum values of the uncertainty analysis for the system performance parameters are presented in Table 3.

5. Results and discussion

The system performance parameters and productivity are expected to be maximized based on the selected new packing pad material (cellulose paper in bee-hive structure) and new design dehumidifier (strips-finned helical coil). The current pad material has higher thermal–hydraulic performance (i.e. highest, heat and mass transfer coefficients and lowest pressure drop) rather than existing ones [45]. Moreover, the current pad material is made of cellulose paper in bee-hive structure that characterizes it to be new, reliable, and most applicable if it was compared with other existing materials [45]. Additionally, the new dehumidifier design is compact and has better heat and mass transfer characteristics in vertical orientation as compared to straight tubes heat exchangers [13]. Therefore, when using an efficient new packing pad humidifier and new design dehumidifier in integrated proposed system then the system performance parameters and productivity will be maximized.

The results of the experimental runs were firstly analyzed and treated to assess and prove that the proposed hybrid HDH and AC system can achieve the function of each sub-system; i.e. can produce fresh water and supply cooling air to remove the heat load of the room and maintain it at the required thermal comfort conditions. The results are then analyzed to study the effects of air and saline water temperatures and flow rates and thickness of cooling pad on the system productivities (fresh water productivity and supply cooling air. The parameters that measure the system performance are then studied and evaluated for the wide ranges

Table 3
Uncertainty of main calculated parameters.

Main Parameters	$\frac{w_{\dot{m}_{FW}}}{\dot{m}_{FW}}$	$\frac{w_{FWR}}{FWR}$	$\frac{w_{COP_{sys}}}{COP_{sys}}$	$\frac{w_{\dot{Q}_R}}{\dot{Q}_R}$	$\frac{w_{\varepsilon_{coil}}}{\varepsilon_{coil}}$	$\frac{w_{\varepsilon_{hum}}}{\varepsilon_{hum}}$	$\frac{w_{TOC}}{TOC}$	$\frac{w_{SCFWP}}{SCFWP}$
Uncertainties	±4.2%	±5.8%	±6.7%	±5.4%	±6.2%	±6.8%	±9.7%	±10.7%

of the studied operating conditions and geometric parameters to find the optimal conditions at which the system has the best performance. The results are then processed to deduce correlations for the productivity and the performance parameters of the system as a function of the operating conditions and the system geometric parameters.

5.1. Proposed system evaluation

Fig. 8 shows the conditions of the supply cooling air (s; state 3) obtained from the system in all the experiments plotted on the Psychrometric chart. The comfort conditions inside the conditioned space (R) is also plotted on the chart. Fig. 8 shows that the supply air temperature obtained in all experiments, whatever the operating conditions and geometric parameters, is always less than the required comfort condition inside the conditioned space (i.e $T_s < T_R$). This proves that the proposed hybrid system is capable to cool the conditioned space removing its sensible heat load. Fig. 8 also shows that humidity of the supply cooling air obtained in most of the experiments is less than that of the humidity of the air inside the room and this proves that the system is capable to extract latent load (vapour) from the conditions space.

It was noticed that the experiments that were conducted at high water and air flow rates in the case of using thick cooling pad produce supply cooling air of higher humidity than that of the conditioned space. In this case the supply air cools and humidify the conditioned space. Such operating conditions of the system is suitable in air conditioning of buildings in hot and dry climates where cooling and humidification are required. Thus it can be concluded that the proposed system can work to cool and dehumidify the air conditioning space as in the case of hot and humid climates or to cool and humidify the air conditioning space as in hot and dry climates. The system operating conditions and geometric parameters must be correctly chosen to satisfy the required case.

Fig. 9 gives the system productivity of the fresh water at different operating and geometric conditions. The figure shows that the proposed hybrid system can produce fresh water for any operating conditions and geometric parameters. Thus the results presented in Figs. 8 and 9 prove that the proposed hybrid system can produce fresh water with space cooling for all the studied operating conditions and geometric parameters and this positively assists that the proposed hybrid system can achieve its purpose (supply fresh water and space cooling) for all the studied operating conditions.

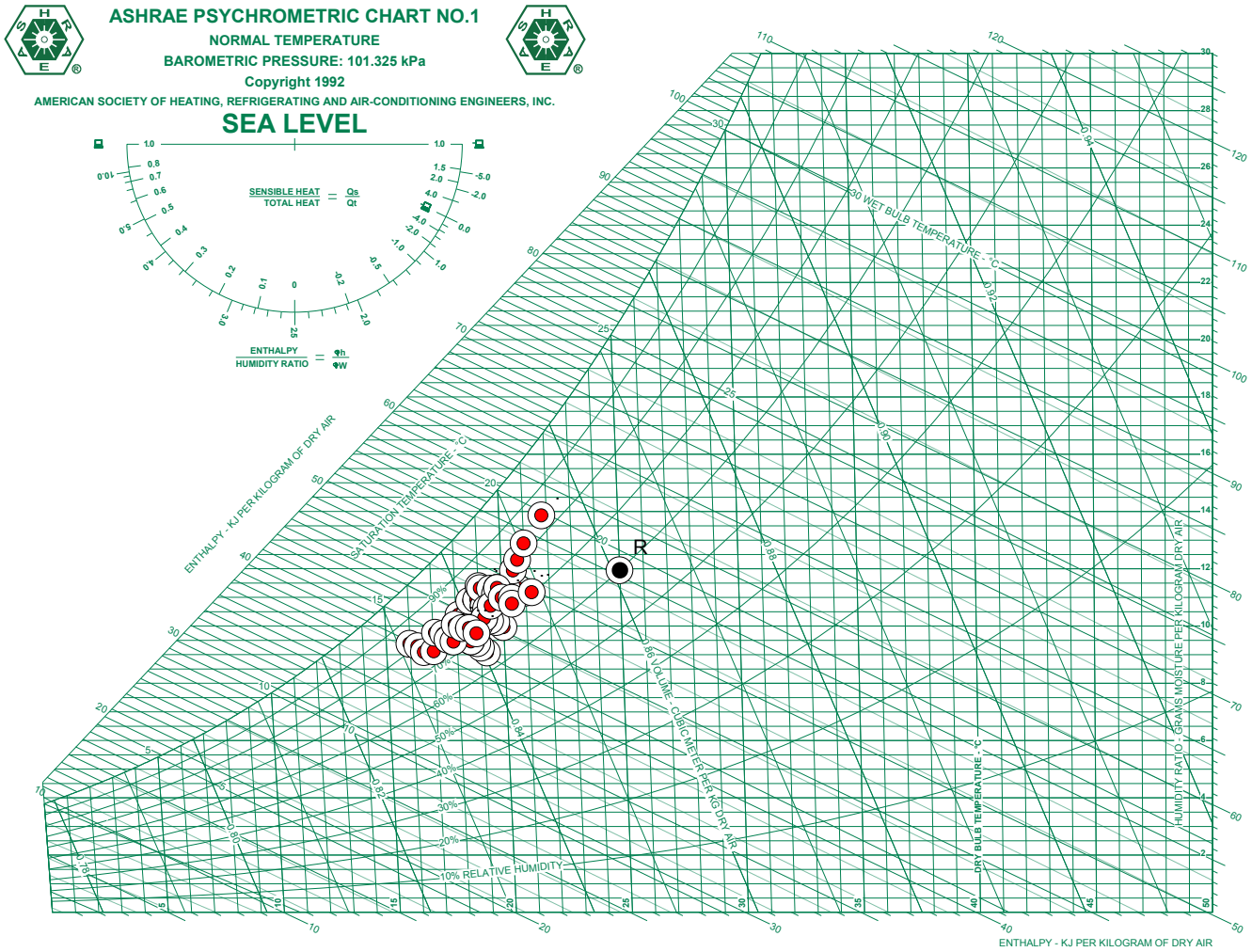

Fig. 8. Space supply air conditions (system evaluation).

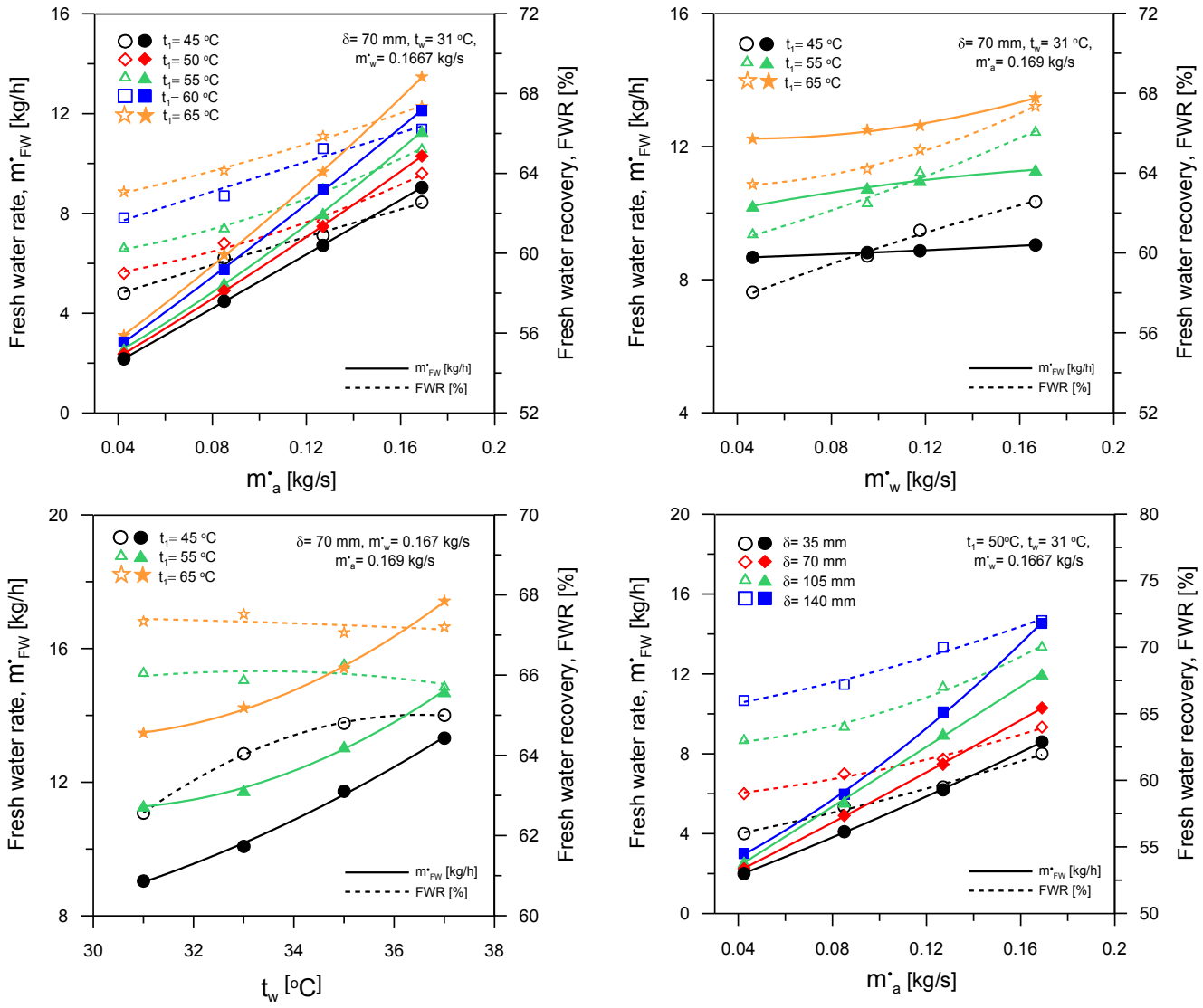

Fig. 9. Effects of air inlet temperature, water temperature & flow rate and pad thickness on fresh water rate and fresh water recovery.

5.2. Parametric study

A parametric study of the effects of air and water flow rates and temperatures and cooling pad thickness on the system productivities (capability of space cooling and fresh water production) and system performance parameters (coefficient of performance and production cost of fresh water) is presented.

5.2.1. Fresh water production rate and water recovery

Effects of air and water temperatures and flow rates at humidifier entrance as well as the effect of cooling pad thickness on fresh water production rate and fresh water recovery are shown in Fig. 9 for all the studied operating conditions and geometric parameters. The figure shows that fresh water productivity and fresh water recovery increases with increasing air and water flow rates and temperature and cooling pad thickness. The reasons of that are (i) the increase of air humidification capacity in humidifier and air dehumidification capacity in cooling coil with rising air and water temperatures, (ii) the increase of the water vapor carried with air by increasing air flow rate causing the increase of water evaporation rate in the humidifier and consequently water dehumidification rate in the cooling coil, (iii) the increase of air to water contact time and contact area in cooling pad by increasing water flow rate and this increases water evaporation rate in the humidifier and consequently the water dehumidification rate in the cooling coil, and (iv) the increase of air to water contact time and contact area in cooling pad by increasing and this increases the humidification capacity of the air which in turn increases the water dehumidification rate in the cooling coil.

Increasing the air humidification capacity in the humidifier and the air dehumidification capacity in the cooling coil increases the fresh water production rate for the same input saline water rate and this causes the increase fresh water recovery. The highest value of $\dot{m}_{FW}$ can be obtained is 17.42 kg/h at $t_1 = 65$ °C, $t_w = 37$ °C, $\delta = 70$ *mm*, $\dot{m}_a =$ 0.169 kg/s and $\dot{m}_w = 0.1667$ kg/s, and the highest FWR is 72% at $t_1 =$ 50 °C, $t_w = 31$ °C, $\delta = 140$ *mm*, $\dot{m}_a = 0.169$ kg/s and $\dot{m}_w = 0.1667$ kg/s, respectively.

5.2.2. Space cooling (supply air temperature and humidity)

Fig. 10 shows the effects of air and water flow rates and temperatures at inlet of the humidifier section as well as effect of cooling pad thickness on space supply air temperature and relative humidity. It is clear from Fig. 10 that decreasing air flow rate, increasing water flow rate, decreasing air and water temperatures and increasing cooling pad section cause the decrease of the supply air temperature. This can be attributed to that (i) for the same water evaporation rate, i.e. the same sensible heat extracted from the air, the temperature of the air decreases

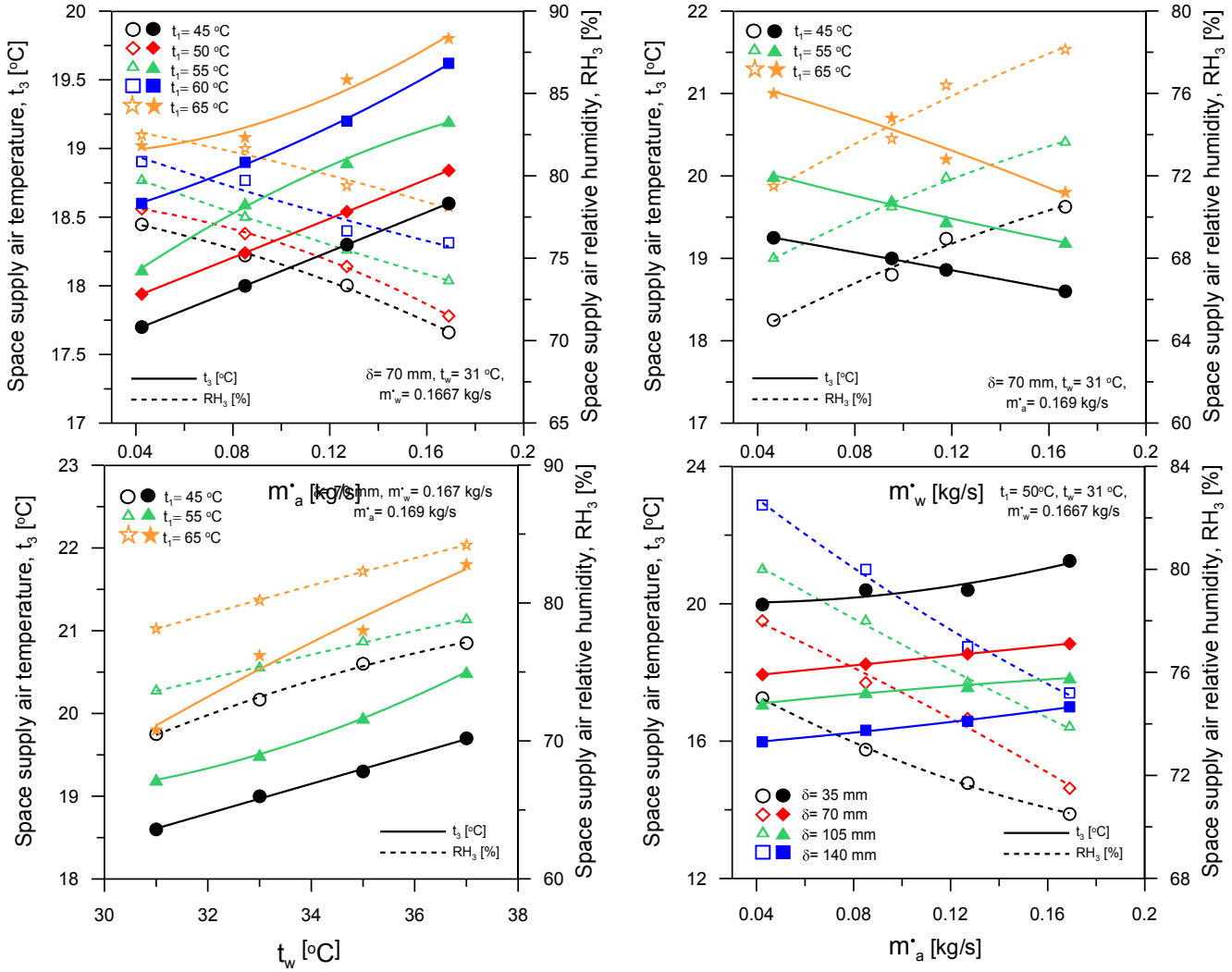

Fig. 10. Effect of air and water temperatures and flow rates and pad thickness on space supply temperature and relative humidity.

with lowering air flow rate, (ii) increasing water flow rate and cooling pad thickness increases the water evaporation rate for the same air flow rate and air inlet temperature and this increases the sensible heat extracted from the air which leads to more reduction in the supply air temperature, and (iii) decreasing the air temperature and the sea water temperature at the inlet to the humidifier system means lower supply temperature for the same water evaporation rate. Decreasing the air and water temperatures causes the decrease of the water evaporation rate and consequently the increase of supply air temperature. This increase in the supply air temperature due to the decrease of the evaporation rate cannot overcome on the decrease of the supply air temperature due to the decrease of air and water inlet temperatures.

Fig. 10 also shows the increase of the supply air relative humidity with the decrease of the air flow rate, the increase of the water flow rate, the increase of the inlet air and water temperatures as well as the increase of the cooling pad thickness. This can be attributed to the increase of the air humidification capacity in the humidifier causing the increase of vapor contents in the air and consequently the increase of the relative humidity of the supply air. Moreover, the proposed system can give space supply air temperature and relative humidity of 16 °C and 82.5%, respectively at $t_1 = 50$ °C, $t_w = 31$ °C, $\delta = 140$ *mm*, $\dot{m}_a = 0.042$ kg/s and $\dot{m}_w = 0.1667$ kg/s.

5.2.3. *Effectiveness of the humidifier and cooling coil*

Fig. 11 illustrates the dependence of the humidifier and cooling-dehumidifying coil effectiveness on air and water flow rates and temperatures and cooling pad thickness. As shown in the figure, the humidifier effectiveness increases with decreasing air flow rate, increasing water flow rate, increasing air and water temperatures, and increasing cooling pad thickness. This is due to the increase of the humidification capacity per kg of dry air which leads to the decrease of the air temperature and consequently the decrease of the air enthalpy at the exit of the humidifier sections. Decreasing the air enthalpy at the exit of the humidifier sections causes the increase of the humidification effectiveness as given by Eq. (5).

Fig. 11 also illustrates the enhancement of the cooling and humidifying coil effectiveness with the decrease of air flow rate, increase of water flow rate, decrease of air and water temperatures and increase of the cooling pad thickness. This can be attributed to that (i) decreasing air flow rate decreases the bypass factor of the coil and increase contact area and contact time of the air with the coil surface leading to the decrease of the exit air temperature and enthalpy (h_3) which cause the increase of coil effectiveness as per Eq. (11), (ii) decreasing air and water temperatures and increasing cooling pad thickness cause the decrease of the supply air temperature (see section 5.2.2 and Fig. 10) and consequently the decrease of air enthalpy at cooling coil exit (h_3) which causes the increase of the coil effectiveness. The maximum values of $\varepsilon_{hum}$and ε_{hum} are 93% at $t_1 = 45$ °C, $t_w = 31$ °C, $\delta = 70$ *mm*, $\dot{m}_a = 0.169$ kg/s and $\dot{m}_w = 0.1667$ kg/s and 86% at $t_1 = 50$ °C, $t_w = 31$ °C, $\delta = 140$ *mm*, $\dot{m}_a = 0.09$ kg/s and $\dot{m}_w = 0.1667$ kg/s), respectively

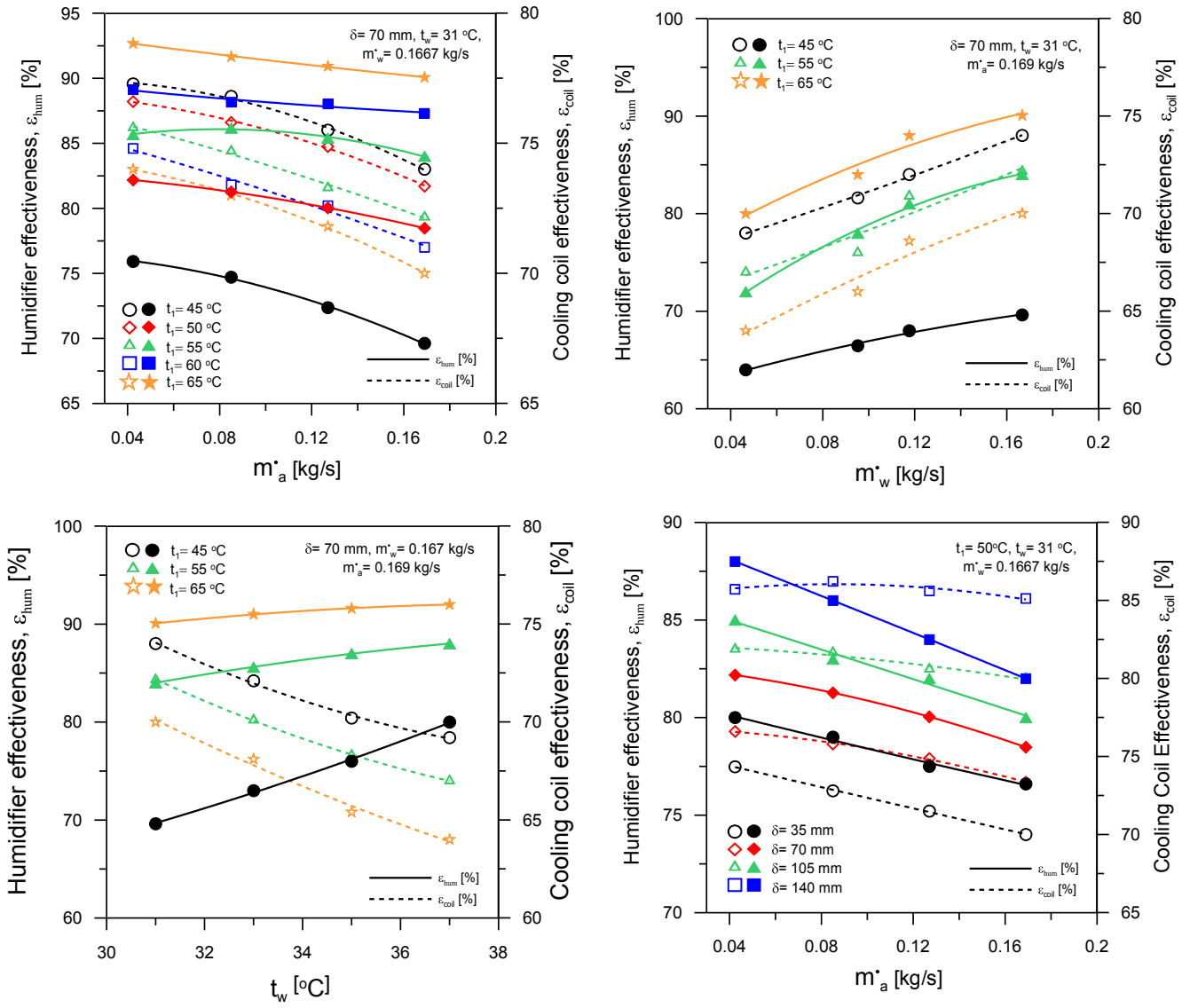

Fig. 11. Effect of air and water temperatures and flow rates and pad thickness on the effectiveness of the humidifier and cooling coil.

5.2.4. Space cooling load and system coefficient of performance

Fig. 12 shows the increase of air capacity to remove space cooling load ($\dot{Q}_R$) with the increase of air and water flow rates and cooling pad thickness and the decrease of air and water temperatures. This may be attributed to the decrease of the temperature of the supply air to the air conditioned space (air temperature at coil exit), as discussed in Section 5.2.3 and shown in Fig. 10, with the increase of air flow and water rates and cooling pad thickness and the decrease of air and water temperatures. Decreasing air supply temperature cause the decrease of supply air enthalpy (h_3) and consequently the increase of the space cooling load as given in Eq. (14)

Fig. 12 also shows the increase of the overall coefficient of performance of the system with the increase of the air and water flow rates and cooling pad thickness and the reduction of air and water temperatures. This is due to the increase of fresh water productivity, fresh water recovery and air cooling capacity which cause the increase of the useful output of the system as shown in Eq. (15). It is worth to mention that increasing air and water flow rates as well as decreasing air and water temperatures cause the increase of the input power to the air fan, water pump and air and water heaters which tend to the decrease of the overall COP of the systems as given in Eq. (15). But the percentage of increase of the system output with the increase of air and water flow rates and cooling pad thickness and the decrease of air and water inlet temperatures is higher than the percentage of increase of the system input powers and the final results is the increase of the overall performance (COP) of the system. The proposed system can reach to pace cooling load of 3.9 kW at $t_1 = 45$ °C, $t_w = 31$ °C, $\delta = 70$ *mm*, $\dot{m}_a = 0.169$ kg/s and $\dot{m}_w = 0.1667$ kg/s and coefficient of performance of 4.35 at $t_1 = 45$ °C, $t_w = 31$ °C, $\delta = 70$ *mm*, $\dot{m}_a = 0.169$ kg/s and $\dot{m}_w = 0.1667$ kg/s.

5.2.5. Total operating cost per day and specific cost of fresh water production

Fig. 13 shows the variation of the daily operating cost ($/day) and the specific cost of the fresh water production (¢/kg_{FW}) with the system operating conditions and geometric parameters. The figure shows the increase of daily operating cost with the increase of air and water flow rates and temperatures at the inlet to the humidifier section and the decrease of the daily operating cost with increasing cooling pad thickness. This may be attributed to (i) the increase of system size and system output with the increase of air and water flow rates as it requires more input power to drive the system as given by Eq. (16), (ii) increasing the air and water temperatures at the inlet of the humidifier section means the increase of the needed power to heat these air and water and consequently the increase of the total operating cost of the system but

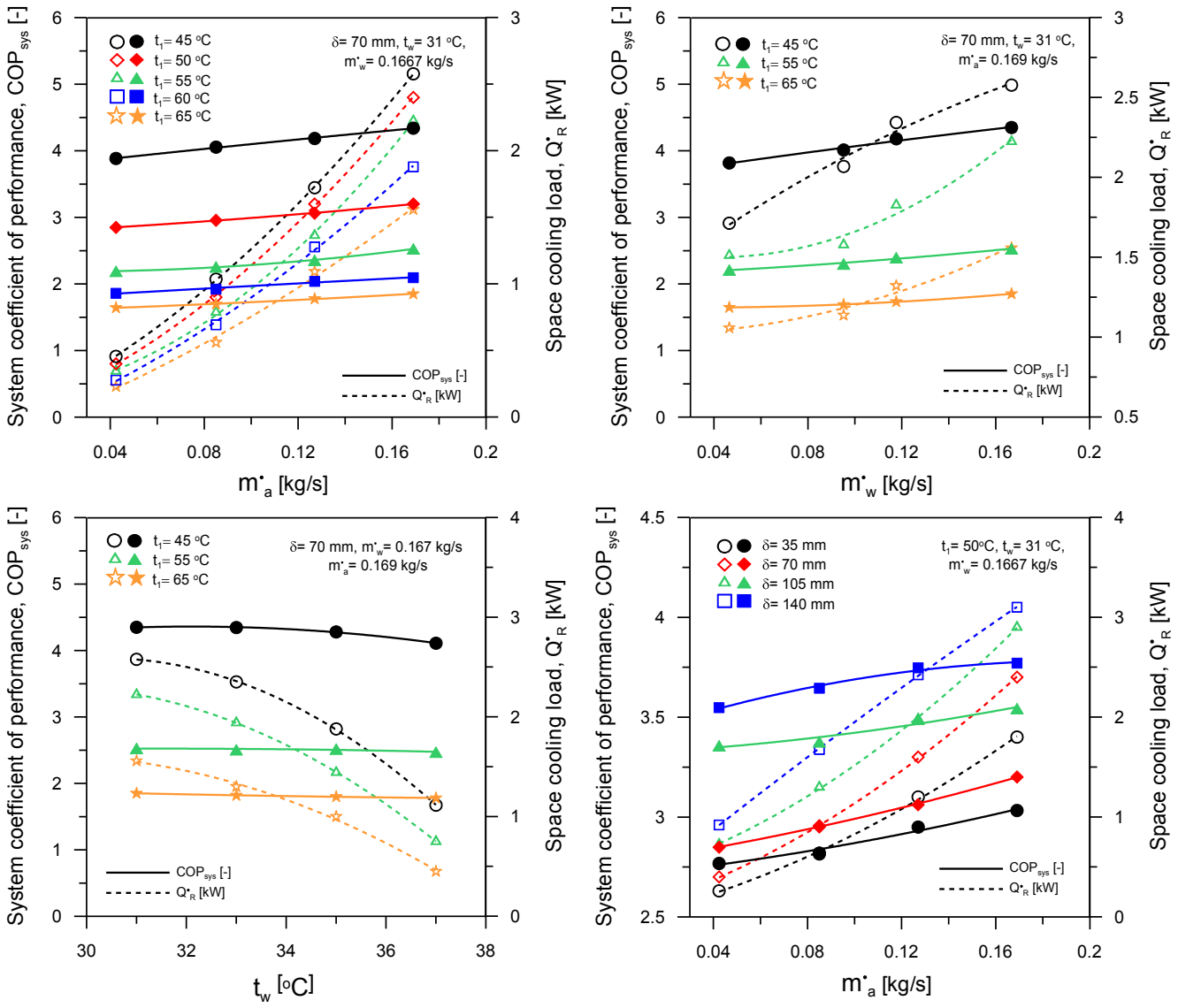

Fig. 12. Effects of air and water temperatures and flow rates and pad thickness on system coefficient of performance and space cooling load.

this is accompanied with the increase of the system output, and (iii) increasing the cooling pad thickness lead to the reduction of the air temperature and air enthalpy at the inlet to the cooling coil and this dramatically decreases the total power of the system in spite of the increase of fan power due increasing cooling pad thickness.

It is better to express the operating cost of the system per kg of the produced fresh water (SCFWP). Fig. 13 shows the decrease of SCFWP with increasing air and water flow rates and cooling pad thickness and the decrease of air and water temperatures at inlet of the humidifier section. This can be attributed to that (i) increasing air and water flow rates increase the fresh water production rate and the input power to the system but the gain in the fresh water production rate is higher than the gain in the input power increase and the final result is the decrease of SCFWP, (ii) increasing the cooling pad thickness decreases the compressor power and the input power to the system and it also increases the fresh water production rate and the final results is a dramatic decrease of the SCFWP, and (iii) decreasing the air and water temperatures at the inlet of the humidifier sections means the decrease of the input power to the air and water heaters but also the decrease of the fresh water production rate. The percentage of the decrease of the heater powers is higher than the percentage of decreasing fresh water production rate and the final result is the decrease of SCFWP. The TOC and *SCFWP* are 0.25 $/day at $t_1 = 65$ °C, $t_w = 31$ °C, $\delta = 70$ *mm*, $\dot{m}_a = 0.04$ kg/s and $\dot{m}_w = 0.1667$ kg/s and 0.7 ¢/kg$_{FW}$ ($t_1 = 45$ °C, $t_w = 31$ °C, $\delta = 70$ *mm*, $\dot{m}_a = 0.169$ kg/s and $\dot{m}_w = 0.1667$ kg/s, respectively.

5.3. Experimental correlations

As shown in section 5.2, water and air flow rates and temperatures and cooling pad thickness strongly affect the system input powers and output as well as the system performance parameters. Accordingly, it is deserved to use the present comprehensive experimental data to deduce experimental correlations that can predict the system outputs and performance parameters in terms of water and air flow rates and temperatures and cooling pad thickness. Table 4 gives the predicted correlations for conditioned space supply air temperature and relative humidity (t_3 and RH_3), fresh water production rate ($\dot{m}_{FW}$), system overall coefficient of performance (COP), cooling load capacity of the supply air ($\dot{Q}_R$), total daily operating cost of the system (TOC) and the cost per kg of fresh water produced (SCFWP) in terms of air and water flow rates and temperatures and cooling pad thickness. Table 4 also gives the errors of these correlations in predicting most of the present experimental data. Fig. 14 also shows the predictions of these correlations compared to the present experimental data. As shown in Table 4

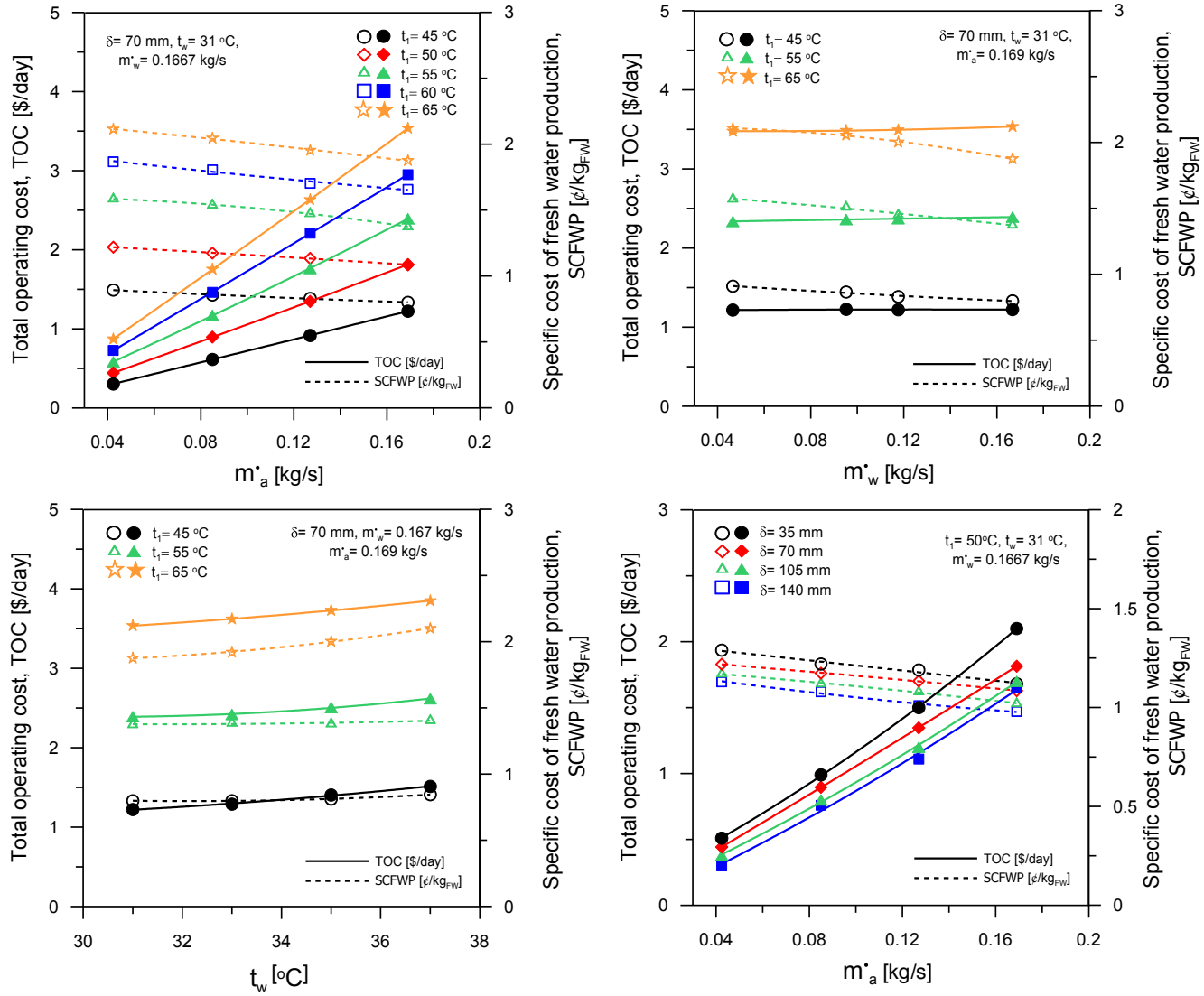

Fig. 13. Effects of air and water temperatures and flow rates and pad thickness on total operating cost per day and specific cost of fresh water production.

Table 4
Experimental correlations prediction and their errors.

Experimental correlations	Error range
$t_3\,[^\circ C] = 3.76(m_a)^{-0.018}(m_w)^{-0.038}(t_1)^{0.153}(t_w)^{0.24}(\delta)^{-0.153}$	Predicts 87% of the experimental results within error ± 15%.
$RH_3\,[\%] = 4.93(m_a)^{-0.024}(m_w)^{-0.038}(t_1)^{0.153}(t_w)^{0.45}(\delta)^{-0.016}$	Predicts 75% of the experimental results within error ± 20%.
$m_{FW}[kg/h] = 0.232(m_a)^{1.075}(m_w)^{0.086}(t_1)^{0.703}(t_w)^{0.95}(\delta)^{0.38}$	Predicts 92% of the experimental results within error ± 10%.
$COP\,[-] = 5829(m_a)^{0.601}(m_w)^{0.08}(t_1)^{-2.24}(t_w)^{0.46}(\delta)^{0.195}$	Predicts 90% of the experimental results within error ± 12%.
$Q_R[kW] = 6.8 \times 10^5(m_a)^{1.17}(m_w)^{0.274}(t_1)^{-1.07}(t_w)^{-1.65}(\delta)^{0.54}$	Predicts 87% of the experimental results within error ± 14%.
$TOC\,[\$/day] = 1.2 \times 10^{-3}(m_a)^{0.935}(m_w)^{-0.082}(t_1)^{1.93}(t_w)^{0.36}(\delta)^{-0.196}$	Predicts 83% of the experimental results within error ± 17%.
$SCFWP\,[¢/kg_{FW}] = 1.2 \times 10^{-4}(m_a)^{-0.094}(m_w)^{-0.134}(t_1)^{2.08}(t_w)^{0.137}(\delta)^{-0.157}$	Predicts 93% of the experimental results within error ± 9%.

and Fig. 14 the deduced correlations can predicts most of the experimental data with acceptable errors of predictions. The presence of such errors can be attributed to the uncertainty of the experimental data as given in Table 3.

5.4. Comparison with previous system

It is worth to compare the fresh water productivity, room cooling load and COP of the proposed hybrid system with other previous HDH-refrigeration/AC hybrid system as given in Table 5. The fresh water productivity and cooling load are mainly depend on the size of the system and the system performance. As the size of the present system and the previous studied systems are different, it is meaningless to compare the numerical values of the fresh water production and the cooling load of the system. However, the table shows that the fresh water productivity, cooling load, and coefficient of performance of the current system are higher than that obtained by Chiranjeevi and Srinivas [56] and Nada et al. [40] for small size systems like the current proposed system. Which proves of using the new packing pad humidifier (cellulose paper in bee-hive structure) and new design dehumidifier (strips-finned helical coil) that maximized the system performance parameters and its productivity within the studied parameters ranges.

Also the trend of variation of the fresh water productivity with the

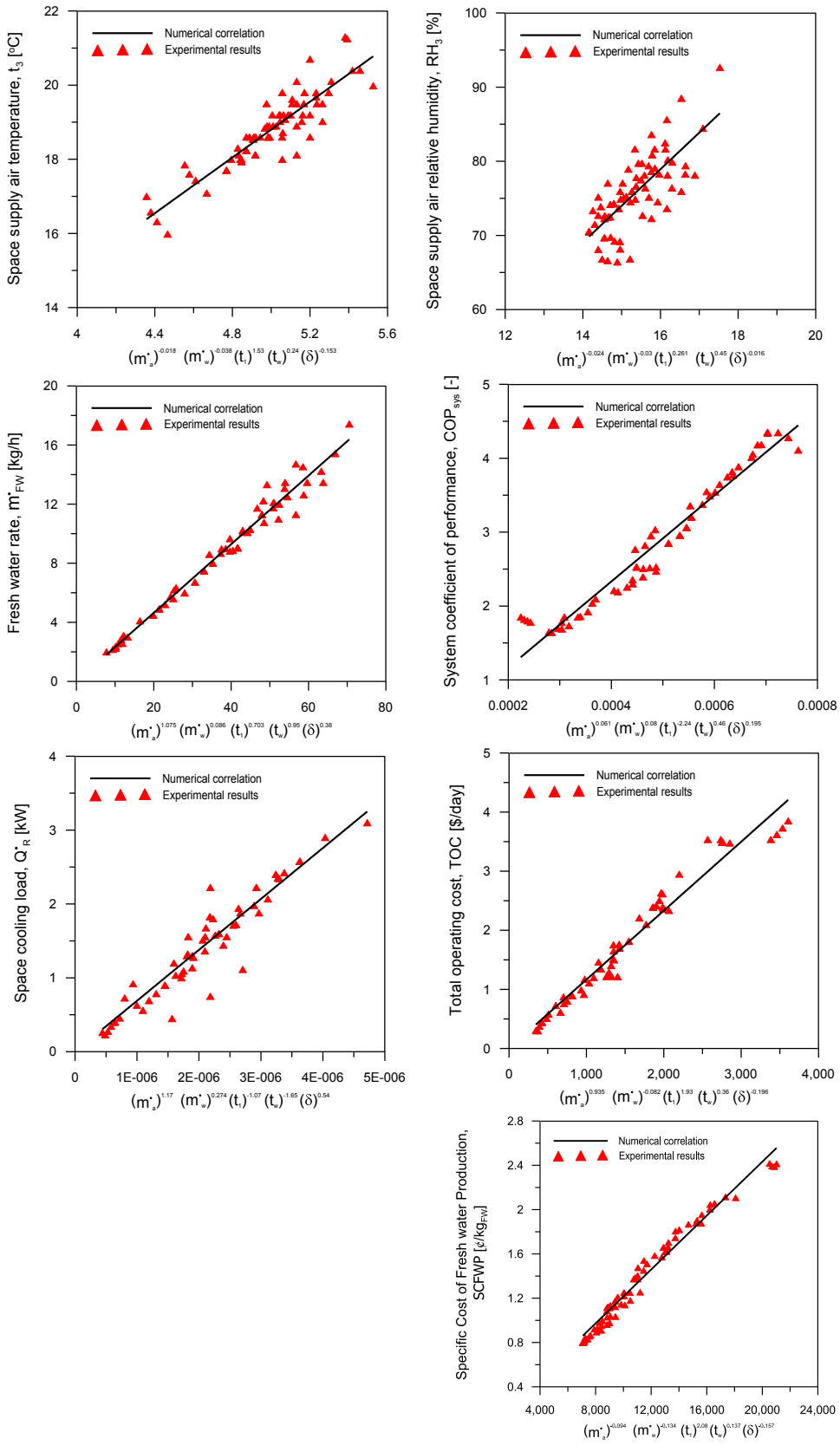

Fig. 14. Experimental correlations prediction of proposed system performance parameters.

Table 5
Comparison of the presented system with other HDH-vapor compression/absorption systems.

Ref.	Type of refrigeration system	Type of study	Water productivity	$\dot{Q}_R$	COP
Chiranjeevi & Srinivas [55]	Vapour absorption	Theoretical	670 kg/h	75 kW	—
Chiranjeevi & Srinivas [56]	Vapour absorption	Experimental & Theoretical	1.5 kg/h	150–200 W	—
Chiranjeevi & Srinivas [57]	Vapour absorption	Theoretical	50 kg/h	200 W	—
Nada et al. [40]	Vapour compression	Experimental	1.77–4.74 kg/h	—	3.214–4.117
Nada et al. [39]	Vapour compression	Theoretical	511.7–11128 kg/h	3516.7 kW	—
Elattar et al. [43]	Vapour compression	Theoretical	69.52–534.1 kg/h	39.72–143.4 kW	1.94–4.152
Fouda et al. [38]	Vapour compression	Theoretical	127.734–501 kg/d	4.076–22.24 kW	2.596–5.092
Current work	**Vapour compression**	**Experimental**	**2.174–17.42 kg/h**	**0.2294–3.9 kW**	**1.648–4.35**

operating conditions was compared with the trends obtained in previous works in Table 5 where the same trend for the effect of air and water temperatures and water flow rates were obtained. Table 5 also shows that the COP of the proposed system lies within the COPs obtained in the previous works that are listed in Table 5.

6. Conclusion

A hybrid HDH and AC system for fresh water production and space cooling is proposed and experimentally examined to confirm that the system is capable to perform its functions. A comprehensive experimental parametric study of the performance of the proposed system was also conducted to find the effects of the system operating conditions and geometric design parameters on the system productivities and performance. The experimental data and results were also used to predict correlations that give the system productivity and performance parameters in terms of the operating conditions and geometric parameters. The results of the study show that:

- The proposed HDH and AC hybrid system can produce fresh water and remove space cooling load to maintain comfort conditions inside the space.
- The system productivity represented by fresh water productivity, cooling load and the low supply air temperature to the cooling space increases by increasing the cooling pad thickness and air and water flow rates and temperatures to the humidifier section.
- The overall coefficient of performance of the system increases with the increase of the air/ water flow rates and cooling pad thickness and the decrease of air/water inlet temperatures.
- The daily production cost of the system increases with increasing inlet air/water flow rates and decreasing cooling pad thickness and air/water temperatures to the humidifier section. Hover, the production cost per kg of fresh water decreases by increasing cooling pad thickness and air and water flow rates and temperatures.
- The empirical correlations obtained from the experimental data can predict the system productivities and system performance parameters within acceptable errors.
- The proposed system can reach to fresh water productivity of 17.42 kg/h at $t_1 = 65$ °C, $t_w = 37$ °C, $\delta = 70$ *mm*, $\dot{m}_a = 0.169$ kg/s and $\dot{m}_w = 0.1667$ kg/s , and pace cooling load of 3.9 kW at $t_1 = 45$ °C, $t_w = 31$ °C, $\delta = 70$ *mm*, $\dot{m}_a = 0.169$ kg/s and $\dot{m}_w = 0.1667$ kg/s.
- Moreover, the proposed system can give space supply air temperature and relative humidity of 16 °C and 82.5%, respectively at $t_1 = 50$ °C, $t_w = 31$ °C, $\delta = 140$ *mm*, $\dot{m}_a = 0.042$ kg/s and $\dot{m}_w = 0.1667$ kg/s.
- Furthermore, the proposed system can attain to coefficient of performance of 4.35 and the lowest specific cost of fresh water production of 0.7 ¢/kg_{FW} at $t_1 = 45$ °C, $t_w = 31$ °C, $\delta = 70$ *mm*, $\dot{m}_a = 0.169$ kg/s and $\dot{m}_w = 0.1667$ kg/s.

Declaration of Competing Interest

The authors declare that they have no known competing financial interests or personal relationships that could have appeared to influence the work reported in this paper.

References

[1] World Health Organization (Ed.), Progress on Drinking Water and Sanitation, 2014.
[2] K. Choon, K. Thu, S. Jin, L. Ang, M. Wakil, A. Bin, Recent developments in thermally driven seawater desalination: energy efficiency improvement by hybridization of the MED and AD cycles, Desalination 365 (2014) 255–270.
[3] J. Uche, L. Serra, L.A. Herrero, A. Valero, JoséAntonio Turégano, C. Torres, Software for the analysis of water and energy systems, Desalination 156 (1-3) (2003) 367–378.
[4] I. Houcine, M. BenAmara, A. Guizani, M. Maâlej, Pilot plant testing of a new solar desalination process by a multiple-effect-humidification technique, Desalination 196 (1-3) (2006) 105–124.
[5] S.A. El-Agouz, A new process of desalination by air passing through seawater based on humidification–dehumidification process, Energy 35 (12) (2010) 5108–5114.
[6] Y.J. Dai, R.Z. Wang, H.F. Zhang, Parametric analysis to improve the performance of a solar desalination unit with humidification and dehumidification, Desalination 142 (2) (2002) 107–118.
[7] G.P. Narayan, M.H. Sharqawy, E.K. Summers, J.H. Lienhard, S.M. Zubair, M. A. Antar, The potential of solar-driven humidification–dehumidification desalination for small-scale decentralized water production, Renew. Sustain. Energy Rev. 14 (4) (2010) 1187–1201.
[8] A.E. Kabeel, E.M.S. El-said, A hybrid solar desalination system of air humidification, dehumidification and water flashing evaporation: part II Experimental investigation, Desalination 341 (2014) 50–60.
[9] A.E. Kabeel, M.H. Hamed, Z.M. Omara, S.W. Sharshir, Experimental study of a humidification-dehumidification solar technique by natural and forced air circulation, Energy 68 (2014) 218–228.
[10] A.E. Kabeel, M.H. Hamed, Z.M. Omara, S.W. Sharshir, Water desalination using a humidification-dehumidification technique - a detailed review, Nat. Resour. 4 (2013) 286–305.
[11] S.A. Nada, Air cooling-dehumidification/desiccant regeneration processes by a falling liquid desiccant film on finned-tubes for different flow arrangements, Int. J. Therm. Sci. 113 (2017) 10–19.
[12] A.S. Huzayyin, S.A. Nada, H.F. Elattar, Air-side performance of a wavy-finned-tube direct expansion cooling and dehumidifying air coil, Int. J. Refrig 30 (2) (2007) 230–244.
[13] S.A. Nada, R. Khater, M.A. Mahmoud, Thermal characteristics enhancement of helical cooling-dehumidifying coils using strips fins, Therm. Sci. Eng. Progr. 16 (2020) 100482, https://doi.org/10.1016/j.tsep.2020.100482.
[14] Y.J. Dai, H.F. Zhang, Experimental investigation of a solar desalination unit with humidification and dehumidification, Desalination 130 (2) (2000) 169–175.
[15] G. Al-Enezi, H. Ettouney, N. Fawzy, Low temperature humidification dehumidification desalination process, Energy Convers. Manage. 47 (4) (2006) 470–484.
[16] N.K. Nawayseh, M.M. Farid, S. Al-Hallaj, A.R. Al-Timimi, Solar desalination based on humidification process—I. Evaluating the heat and mass transfer coefficients, Energy Convers. Manage. 40 (13) (1999) 1423–1439.
[17] C. Muthusamy, K. Srithar, Energy and exergy analysis for a humidification–dehumidification desalination system integrated with multiple inserts, Desalination 367 (2015) 49–59.
[18] C. Yamalı, I. Solmus, A solar desalination system using humidification–dehumidification process: experimental study and comparison with the theoretical results, Desalination 220 (2008) 538–551.
[19] J. Orfi, M. Laplante, H. Marmouch, N. Galanis, B. Benhamou, S.B. Nasrallah, C. T. Nguyen, Experimental and theoretical study of a humidification-dehumidification water desalination system using solar energy, Desalination 168 (2004) 151–159.
[20] S. Al-Hallaj, M.M. Farid, A. Rahman Tamimi, Solar desalination with a humidification-dehumidification cycle: performance of the unit, Desalination 120 (3) (1998) 273–280.

[21] H.A. Ahmed, I.M. Ismail, W.F. Saleh, M. Ahmed, Experimental investigation of humidification-dehumidification desalination system with corrugated packing in the humidifier, Desalination 410 (2017) 19–29.
[22] W.F. He, J.J. Chen, D. Han, L.T. Luo, X.C. Wang, Q.Y. Zhang, S.Y. Yao, Energetic, entropic and economic analysis of an open-air, open-water humidification dehumidification desalination system with a packing bed dehumidifier, Energy Convers. Manag. 199 (2019), 112016.
[23] W. He, H. Yang, D. Han, Thermodynamic investigation and optimization of a heat pump coupled open-air, open-water humidification dehumidification desalination system with a direct contact dehumidifier, Desalination 469 (2019), 114101.
[24] S.A. Nada, A. Fouda, M.A. Mahmoud, H.F. Elattar, Experimental investigation of energy and exergy performance of a direct evaporative cooler using a new pad type, Energy Build. 203 (2019), 109449.
[25] Narmine H. Aly, Adel K. El-Figi, Mechanical vapor compression desalination systems, Desalination 158 (2003) 143–150.
[26] Y. Ghalavand, M.S. Hatamipour, A. Rahimi, Humidification compression desalination, Desalination 341 (2014) 120–125.
[27] A. Giwa, H. Fath, S.W. Hasan, Humidification–dehumidification desalination process driven by photovoltaic thermal energy recovery (PV-HDH) for small-scale sustainable water and power production, Desalination 377 (2016) 163–171.
[28] A.E. Kabeel, E.M.S. El-Said, A hybrid solar desalination system of air humidification dehumidification and water flashing evaporation: A comparison among different configurations, Desalination 330 (2013) 79–89.
[29] P. Gao, L. Zhang, H. Zhang, Performance analysis of a new type desalination unit of heat pump with humidification and dehumidification, Desalination 220 (1-3) (2008) 531–537.
[30] M. Mehrgoo, M. Amidpour, Constructal design and optimization of a direct contact humidification–dehumidification desalination unit, Desalination 293 (2012) 69–77.
[31] A.M.I. Mohamed, N.A. El-Minshawy, Theoretical investigation of solar humidification–dehumidification desalination system using parabolic trough concentrators, Energy Convers. Manage. 52 (10) (2011) 3112–3119.
[32] M.T. Ghazal, U. Atikol, F. Egelioglu, An experimental study of a solar humidifier for HDD systems, Energy Convers. Manage. 82 (2014) 250–258.
[33] A.S. Nafey, H.E.S. Fath, S.O. El-Helaby, A.M. Soliman, Solar desalination using humidification dehumidification processes. Part I. A numerical investigation, Energy Convers. Manage. 45 (7-8) (2004) 1243–1261.
[34] A.S. Nafey, H.E.S. Fath, S.O. El-Helaby, A. Soliman, Solar desalination using humidification–dehumidification processes. Part II. An experimental investigation, Energy Convers. Manage. 45 (7-8) (2004) 1263–1277.
[35] Adel M. Abdel Dayem, M. Fatouh, Experimental and numerical investigation of humidification-dehumidification solar water desalination systems, Desalination, 247 (2009) 594–609.
[36] C. Yıldırım, İ. Solmuş, A parametric study on a humidification–dehumidification (HDH) desalination unit powered by solar air and water heaters, Energy Convers. Manage. 86 (2014) 568–575.
[37] S.W. Sharshir, G. Peng, N. Yang, M.O.A. El-Samadony, A.E. Kabeel, A continuous desalination system using humidification – dehumidification and a solar still with an evacuated solar water heater, Appl. Therm. Eng. 104 (2016) 734–742.
[38] A. Fouda, S.A. Nada, H.F. Elattar, S. Rubaiee, A. Al-Zahrani, Performance analysis of proposed solar HDH water desalination systems for hot and humid climate cities, Appl. Therm. Eng. 144 (2018) 81–95.
[39] S.A. Nada, H.F. Elattar, A. Fouda, Performance analysis of proposed hybrid air conditioning and humidification–dehumidification systems for energy saving and water production in hot and dry climatic regions, Energy Convers. Manage. 96 (2015) 208–227.
[40] S.A. Nada, H.F. Elattar, A. Fouda, Experimental study for hybrid humidification–dehumidification water desalination and air conditioning system, Desalination 363 (2015) 112–125.
[41] G. Yuan, L. Zhang, H. Zhang, Experimental research of an integrative unit for air-conditioning and desalination, Desalination 182 (1-3) (2005) 511–516.
[42] A. Fouda, S.A. Nada, H.F. Elattar, An integrated A/C and HDH water desalination system assisted by solar energy: Transient analysis and economical study, Appl. Therm. Eng. 108 (2016) 1320–1335.
[43] H.F. Elattar, A. Fouda, S.A. Nada, Performance investigation of a novel solar hybrid air conditioning and humidification–dehumidification water desalination system, Desalination 382 (2016) 28–42.
[44] S.A. Nada, H.F. Elattar, A. Fouda, Energy-efficient hybrid A/C and freshwater production system proposed for high latent load spaces, Int. J. Energy Res. 43 (13) (2019) 6812–6826.
[45] S.A. Nada, H.F. Elattar, M.A. Mahmoud, A. Fouda, Performance enhancement and heat and mass transfer characteristics of direct evaporative building free cooling using corrugated cellulose papers, Energy 211 (2020), 118678.
[46] TABREED, Cooling Cell Pads, <http:// www.tabreedcoolingpads.com> (accessed on 03.05.2019).
[47] P. Martínez, J. Ruiz, P.J. Martínez, A.S. Kaiser, M. Lucas, Experimental study of the energy and exergy performance of a plastic mesh evaporative pad used in air conditioning applications, Appl. Therm. Eng. 138 (2018) 675–685.
[48] R.W. Koca, W.C. Hughes, L.L. Christianson, Evaporative cooling pads: test procedure and evaluation, Appl. Eng. Agric. 7 (4) (1991) 485–490.
[49] T. Gunhan, V. Demir, A.K. Yagcioglu, Evaluation of the Suitability of Some Local Materials as Cooling Pads, Biosyst. Eng. 96 (3) (2007) 369–377.
[50] A. Malli, H.R. Seyf, M. Layeghi, S. Sharifian, H. Behravesh, Investigating the performance of cellulosic evaporative cooling pads, Energy Convers. Manage. 52 (7) (2011) 2598–2603.
[51] A. Franco, D.L. Valera, A. Madueño, A. Peña, Influence of water and air flow on the performance of cellulose evaporative cooling pads used in mediterranean greenhouses, Trans. ASABE 53 (2) (2010) 565–576.
[52] G.P. Narayan, M.H. Sharqawy, J.H. Lienhard V, S.M. Zubair, Thermodynamic analysis of humidification dehumanization desalination cycles, Desalin. Water Treat. 16 (2010) 339–353.
[53] Mostafa H. Sharqawy, Mohamed A. Antar, Syed M. Zubair, Abubaker M. Elbashir, Optimum thermal design of humidification dehumidification desalination systems, Desalination 349 (2014) 10–21.
[54] Robert J. Moffat, Describing the uncertainties in experimental results, Exp. Therm Fluid Sci. 1 (1) (1988) 3–17.
[55] C. Chiranjeevi, T. Srinivas, Combined two stage desalination and cooling plant, Desalination 345 (2014) 56–63.
[56] C. Chiranjeevi, T. Srinivas, Experimental and simulation studies on two stage humidification–dehumidification desalination and cooling plant, Desalination 376 (2015) 9–16.
[57] C. Chiranjeevi, T. Srinivas, Augmented desalination with cooling integration, Int. J. Refrig 80 (2017) 106–119.